DYNAMICS OF PHASE SLIP CENTERS AND HOT SPOTS IN SUPERCONDUCTING NIOBIUM STRIPS

FANDI OKTASENDRA

PHYSICS

MAY, 2015

DYNAMICS OF PHASE SLIP CENTERS AND HOT SPOTS IN SUPERCONDUCTING NIOBIUM STRIPS

BY

FANDI OKTASENDRA

A Thesis Presented to the

DEANSHIP OF GRADUATE STUDIES

KING FAHD UNIVERSITY OF PETROLEUM & MINERALS

DHAHRAN, SAUDI ARABIA

In Partial Fulfillment of the

Requirements for the Degree of

MASTER OF SCIENCE

In

PHYSICS

MAY, 2015

KING FAHD UNIVERSITY OF PETROLEUM & MINERALS
DHAHRAN 31261, SAUDI ARABIA

DEANSHIP OF GRADUATE STUDIES

This thesis, written by **FANDI OKTASENDRA** under the direction of his thesis adviser and approved by his thesis committee, has been presented to and accepted by the Dean of Graduate Studies, in partial fulfillment of the requirements for the degree of **MASTER OF SCIENCE IN PHYSICS**.

Thesis Committee

Dr. Khalil Harrabi (Adviser)

Prof. Hocine Bahlouli (Member)

Prof. Khalil Ziq (Member)

Dr. Shankar Kunwar (Member)

Dr. Muhammad Baseer Haider (Member)

Dr. Abdullah A. Al-Sunaidi
Department Chairman

Dr. Salam A. Zummo
Dean of Graduate Studies

21/5/15
Date

This thesis is dedicated to my beloved parents, brothers and sister

ACKNOWLEDGMENTS

All prise and thanks to Almighty Allah who gave me the courage to accomplish this thesis work. In addition, I would like to express my gratitude to all people who gave their support, commitment, and kindness to me in completing my M.S. degree in the physics department of King Fahd University of Petroleum and Minerals. But first, I gratefully acknowledge the KFUPM for their support to my thesis work through a DSR project.

My special appreciation goes to my advisor, Dr. Khalil Harrabi, for his motivation, encouragement, patience, and expert guidance throughout my thesis work. His invaluable constructive comments and suggestions guided not only my thesis work and but also my path through life.

I am indebted to my thesis committee members: Prof. Hocine Bahlouli, Prof. Khalil Ziq, Dr. Shankar Kunwar, and Dr. Muhammad Baseer Haider, for their careful evaluation and suggestive comments of my work. I especially thank Prof. Hocine Bahlouli for his encouragements and helpful discussion on the theoretical part of my thesis. I also especially thank Prof. Khalil Ziq for his advices, helpful discussion, and allowing me to use some of his instruments during my experimental

work. I also thank him for giving me an invaluable research experience through one of his project on my first year of study here.

I would like to express my sincere appreciate to the current and former chairmans of the Physics Department for the all facilities and supports on my academic affair. I would also like to thank all faculty of the Physics Department for the immense knowledge extended to me. My special thanks go to Dr. Mohammed M. Faiz for lending me Tinkham's textbook of Introduction to Superconductivity which was very helpful in understanding the concepts of superconductivity.

I would not forget to express my sincere thanks to all staff of the Physics Department for their help and assistance during my study. I especially thank Mr. Abdullah for his help during my experimental work.

I would like to thank to all my colleagues and friends in the Physics Department for their moral support and suggestions. My special thanks go to all my friends in the Indonesian student community for their support, suggestion and encouragement during my study. Thanks for the friendship and memories.

The last but surely not the least, my deepest gratitude goes to my beloved parents, brothers and sister for their consistent and persistent support and prayers.

TABLE OF CONTENTS

LIST OF TABLES

LIST OF FIGURES

THESIS ABSTRACT

NAME:	Fandi Oktasendra
TITLE OF STUDY:	Dynamics of Phase Slip Centers and Hot Spots in Superconducting Niobium Strips
MAJOR FIELD:	Physics
DATE OF DEGREE:	May, 2015

This thesis is focused on the study of the destruction of superconductivity caused by an electrical current pulse in niobium superconducting thin film strips at different temperatures. For this purpose, our experimental work consisted in applying nanosecond current pulses from the signal generator to the film strips via a 50 Ω coaxial cable. A 250 ns delay line was used to separate the incident pulse from the reflected one. The voltage response of the film was measured by a fast oscilloscope via lateral probes of the sample with 187 Ω resistance connected in series. Below the critical temperature T_c, applying a current larger than the critical current I_c results in dissipative regions in the sample which can be interpreted either as phase slip centers (PSC) or normal hot spot (HS). Both dissipative modes are found to appear after some delay time, t_d. The time dependent Ginzburg-Landau (TDGL)

theory can be used to fit the delay time as a function of the reduced current I/I_c giving the gap relaxation time τ_d from which we can deduce the phonon escape time. We found, for niobium films, that the heat escape time is independent of the temperature in the Debye regime. In addition, we have estimated the temperature reached inside the resistive states.

ملخص الرسالة

الاسم الكام: فاندي أكتاسيندرا

عنوان الرسالة: **ديناميكية المركز الزلقة والنقاط الساخنة في أغشية النيوبيوم المفرطة التوصيل**

التخصص: فيزياء

تاريخ الدرجة: مايو، ٢٠١٥

تعنى هذه الأطروحة بدراسة تدمير خاصية فرط التوصيل في شرائح النيوبيوم الرقيقة عند درجات حرارة مختلفة والناتجة عن تيار كهربائي نبضي. لهذا الغرض، قمنا بتطبيق نبضة كهربائية ذات زمن دوري نانوي (نانو ثانية) باستخدام مولد للنبضات وتوصيلها الى أغشية النيوبيوم الرقيقة عن طريق أسلاك محورية مقاومتها تساوي ٥٠ أوم. ولإحداث تأخير ما بين النبضة الكهربائية الساقطة على الشرائح الرقيقة والمنعكسة منها تم استخدام اسلاك محورية تقوم بفصل النبضتين بزمن مقداره ٢٥٠ نانو ثانية. تم قياس فرق الجهد الناتج في الشريحة عن طريق جهاز راسم الذبذبات. كما تم وصل نقاط التوصيل التي على الأغشية مع مقاومة مقدارها ١٨٧ أوم على التوالي ومن ثم توصيلها مع جهاز راسم الذبذبات. لقد لوحظ عند درجات الحرارة التي اقل من درجة الحرارة الحرجة والتي تكون عندها الشريحة في حالة فرط التوصيل وعندما تكون شدة التيار اكبر من شدة التيار الحرج تكونت على شريحة النيوبيوم مناطق تبديد للطاقة يمكن تفسيرها على أنها مراكز زلقة أو نقاط ساخنة تبدأ في الظهور بعد زمن تأخير(t_d). ستخدمنا نظرية جينزبرغ-لانداو التي تعتمد على الزمن لموائمة التغير في زمن التأخير مع التيار الحرج للحصول على زمن الاسترخاء (τ_d) والذي بدوره يعطينا زمن افلات الفونونات. وجدنا أن زمن افلات الحرارة لا يعتمد على درج الحرارة وذلك ضمن مدى ديباي الحراري. كما قمنا بتقدير درجة الحرارة داخل هذه المراكز.

CHAPTER 1

INTRODUCTION

1.1 History of superconductivity

Superconductivity was discovered by a Dutch physicist, Kamerlingh Onnes, in 1911 [1], after he successfully liquefied helium. When he cooled down a tube of mercury to a temperature of about 4.2 K, he observed that its electrical resistivity dropped drastically down to zero below a certain temperature, known as the critical temperature T_c. This zero-electrical resistance has become the most outstanding property of superconductors. The fact that it is a real disappearance of the resistivity was confirmed by the experiment of persistent currents circulating in a superconducting ring. This experiment showed that the currents can, in principle, flow in the superconductor without measurable reduction for a long time (a record appears to be 2.5 years [2]).

One property of superconductiviy is called the perfect diamagnetism *i.e.* a superconducting material behaves as a perfect diamagnet. This phenomenon was

discovered by Meissner and Ochsenfeld in 1933. They found that not only a magnetic field is excluded from entering a superconductor but also a magnetic field in the normal state is expelled as the superconductor is cooled below T_c. This phenomenon is then called the Meissner effect. The expulsion of magnetic field in the superconductor implies that the superconductivity is destroyed by a critical magnetic field H_c. It was found empirically that H_c is temperature dependent. The temperature dependence of H_c is well approximated by a parabolic law as illustrated in Fig. 1.1.

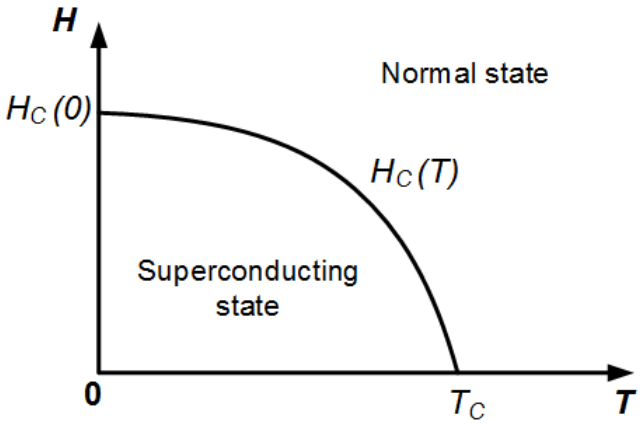

Figure 1.1: Critical magnetic field as a function of temperature.

This figure shows that there is a certain critical magnetic field above which superconductivity breaks down. Furthermore, because magnetic field is linearly proportional to the current this also means that there is a critical current (I_c) above which the superconductivity breaks down. However, the temperature dependence of current is not always able to be depicted similarly to the magnetic field-temperature dependence. The value of the critical current depends on the nature and geometry of the superconducting material. It is related to whether the

magnetic field produced by the current exceeds the critical field at the surface of the superconductor .

1.2 Elementary phenomenological theories

1.2.1 London's equation

In 1935, the London's brothers, F. and H. London, described the properties of superconductivity, *i.e.* perfect conductivity and perfect diamagnetism, by proposing the following equation to govern the microscopic electric field $\vec{E}$ and magnetic field h in superconductors:

$$E = \frac{\partial}{\partial t}\left(\Lambda J_s\right), \tag{1.1}$$

$$h = -c \cdot \operatorname{curl}\left(\Lambda J_s\right) \tag{1.2}$$

where

$$\Lambda = \frac{4\pi\lambda^2}{c^2} = \frac{m}{n_s e^2} \tag{1.3}$$

Λ is a phenomenological parameter and λ is known as a London penetration depth over which the magnetic field is exponentially suppressed. J_s and n_s are the superconducting current and electrons densities, respectively. Eq. (1.1) implies that the electric field accelerates superconducting electrons rather than sustaining their velocity against resistance as happened in a normal metal. Thus this

equation can describe the perfect conductivity property of superconductivity. Eq. (1.2), if combined with the Maxwell equation $\nabla \times h = 4\pi J/c$, describes the decaying of magnetic field exponentially from the exterior of the sample over the distance of penetration depth λ.

1.2.2 Ginzburg-Landau theory

Another important theory that governs the electrodynamic of superconductivity was proposed by Ginzburg and Landau in 1950. It describes the superconducting electrons as a pseudo-wavefunction ψ such that $n_s = |\psi|^2$ [3], where n_s is the density of superconducting currents. This theory is based on Landau's general theory of 2^{nd} order phase transition. The pseudo-wavefunction ψ obeys the differential equation

$$\frac{1}{2m*}\left(\frac{\hbar}{i}\nabla - \frac{e*}{c}A\right)^2 \psi + \beta|\psi|^2\psi = -\alpha\left(T\right)\psi \tag{1.4}$$

where α and β are the expansion coefficients. The Ginzburg-Landau equation lead to two characteristic lenghts, namely the G-L penetration depth, $\lambda_{GL} = \sqrt{(m\beta/4\mu_0 e^2\,|\alpha|)}$ and the coherence lenght, $\xi = \sqrt{(\hbar^2/2m\,|\alpha|)}$ where α is directly proportional to $(T - T_c)$ and β is independent of T. The coherence length ξ can be described as a minimum distance over which the superconducting order parameter $\psi(r)$ can be varied without breaking the superconductivity.

1.2.3 Bardeen-Cooper-Schrieffer theory

In 1957, Bardeen, Cooper, and Schrieffer (BCS) made a remarkably revolution in the theory of superconductivity where they produced a theory to explain the origin of superconductivity. Later on, it could also explain other properties of superconductivity such as zero resistance, perfect diamagnetism, flux quantization, etc. The theory is known as the BCS theory.

In the BCS theory [4], it is shown that, in the presence of phonons, there is a net attractive interaction between electrons in the neighborhood of the Fermi surface. This attractive interaction is viewed as an exchange of phonons (the quanta of lattice vibration energy) and result in the formation of a pair of electron, known as *Cooper pairs*. Two electrons are bounded together and constrained to remain near each other as they move through the metal. The property of Cooper pair is that they have equal and opposite momentum and spin. Therefore they can take the character of a boson and condensate into the ground state.

1.3 Type I and type II superconductors

Based on the way the applied magnetic field penetrates the material and changes the superconducting state to the normal state, superconductors are divided into two groups known respectively as type I and type II superconductors. The difference between the two types of superconductor is illustrated in Fig. 1.2.

In type I superconductors, there is no penetration flux below a critical field H_c that increases as T goes down below T_c. When the applied magnetic field exceeds

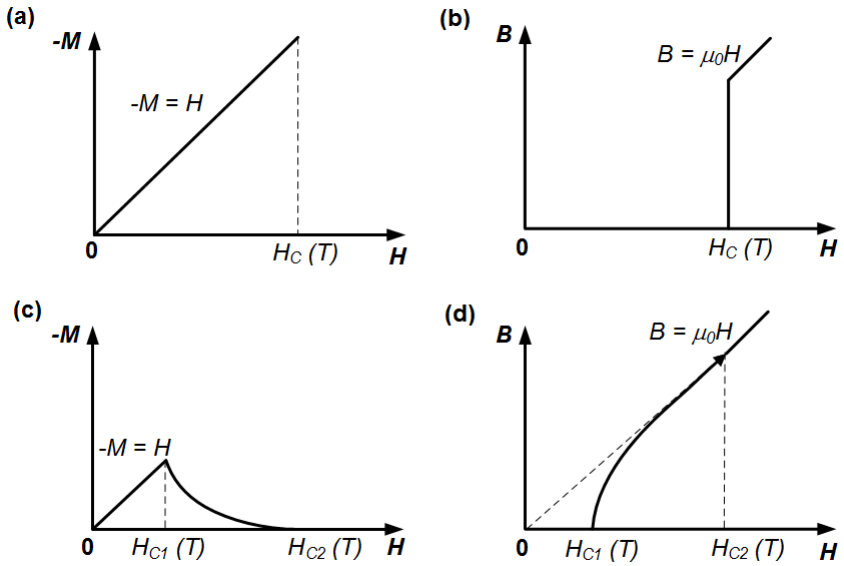

Figure 1.2: Schematic of magnetization curve of type I (a and b) and type II (c and d) superconductors. Type I: (a) Below H_c, the diamagnetic magnetization $M = -H$. Above H_c, M drops to zero. (b) Below H_c, there is no magnetic field penetration (B = 0). Above H_c, magnetic field penetrates perfectly. Type II: (c) Below H_{c1}, $M = -H$. Between H_{c1} and H_{c2}, M falls smoothly to zero. (d) Below H_{c1}, no magnetic field penetrates (B = 0). Between H_{c1} and H_{c2}, magnetic field rises smoothly to $B = \mu_0 H$.

H_c the superconducting material returns back to the normal state and the field penetrates perfectly. The same behavior also occurs in type 2 superconductors below a lower critical field H_{c1}. But, when the applied field exceeds the lower critical field H_{c1} and is less than an upper critical field H_{c2}, where $H_{c2} > H_{c1}$, there is a partial penetration of magnetic flux and the sample exhibits a rather complicated microscopic structure in both normal and superconducting regions, known as the mixed state. Once the applied field exceeds H_{c2}, the superconducting material returns back to the normal state and the field completely penetrates the material.

1.4 Resistive modes in superconducting filament

The existance of a superconducting state is characterized by three main parameters: the critical temperature T_c, the critical magnetic field H_c, and the critical current I_c. Exceeding one of these parameters results in the breakdown of superconductivity. The current-induced breakdown of superconductivity in superconducting material has attracted a lot of attention since it involves fundamental phenomena and advanced concepts such as dissipative mechanisms including phase slips centers, hot spots, vortices, etc. These are some mechanisms which are responsible for creating the resistive states in superconducting material.

When a current in a long quasi-one dimensional superconducting filament with transverse dimension comparable to the Ginzburg-Landau coherence length is biased slightly above the critical current, the superconducting state generally does not represent fully the normal conducting state but exhibits a finite resistance. It was found initially in a tin whisker that a resistive state was observed at temperatures just below T_c as the appearance of regular steplike structures in the I-V characteristics [5, 6] (Fig. 1.3). These were interpreted as phase slip centers (PSCs) [7]. At some other regime of temperatures far below T_c, it was reported that resistive state develops across a spatially localized hot spot (HS) maintained in the normal state by Joule heating (the process of heat releasing due to the flow of electron in the normal state) [8].

In Fig. 1.3, the voltage increases linearly with the increasing of current at temperature larger than the critical temperature, $T > T_c$ as the filament is in

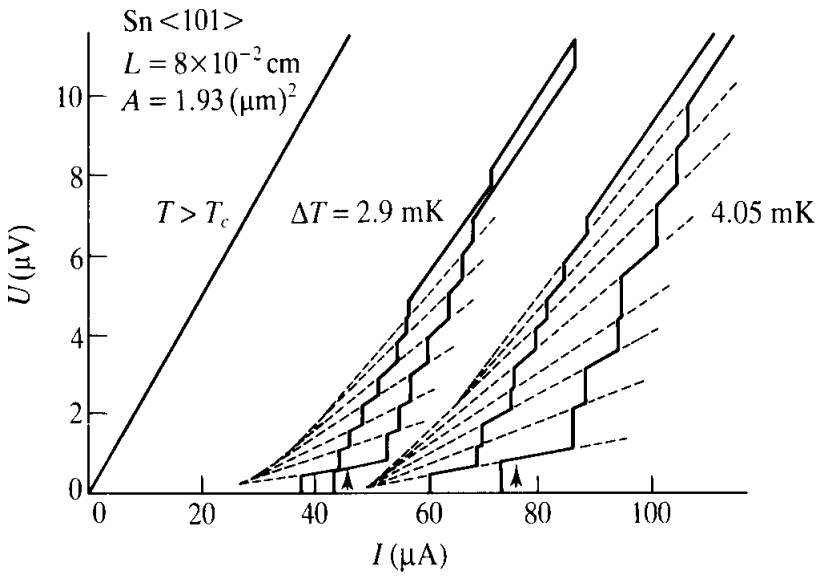

Figure 1.3: Current-voltage characteristics of whiskers showing regular steps structure of phase slip centers (PSCs) [6].

the normal state. At temperature less than T_c, for instance $\Delta T = T - T_c = 2.9$ mK, the voltage appears as a jump after the current is increase above the critical current. This jump of voltage is attributed as the formation of a PSC. The voltage increases linearly as the current is increased further more. When another PSC is formed in somewhere else of the filament, the voltage shows another jump. These steps are created until the whole filament becomes a normal metal so that the voltage increases linearly as it does in the normal state. It can be seen that each successive jumps adds the same amount to the differential resistance, $\frac{\mathrm{d}U}{\mathrm{d}I}$. The slope of each voltage intersects the current axis at the same value known as the superconducting excess current. The same behavior is also seen at lower temperature ($\Delta T = 4.05$ K).

The term "phase slip" was initially introduced by W. A. Little in 1967 when he studied the decay of persistent current in quasi-1D structure materials [9].

He related the appearance of the step structure in the I-V characteristics to the successive appearence of localized structures ("phase-slip centers"). Following the theory of Langer and Ambegaokar [7], the phenomenon of phase slip center can be understood by considering two points x_1 and x_2 of a superconducting filament with potential $V(t)$ (Fig. 1.4). The phase difference of the superconducting order parameter is given by the Josephson relation

$$\frac{d\varphi_{12}}{dt} = \frac{2eV(t)}{\hbar} \tag{1.5}$$

where φ_{12} is the phase difference of the two ends, e is the electron charge, and $\hbar$ is the reduced Planck constant.

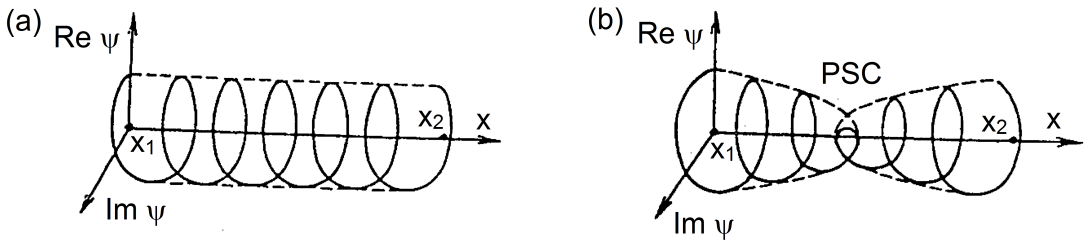

Figure 1.4: Illustration of phase-slip center creation in a 1D superconducting filament along the x-axis. Im ψ and Re ψ are the imaginary and real parts of the superconducting order parameter; (a) in the superconducting state and (b) when a phase-slip center is created [3].

If $V(t) > 0$ then the phase difference increases with time. This leads to an increase of $\nabla\varphi(x)$ followed by the increasing of supercurrent velocity, $v_s = (\hbar/m)\nabla\varphi(x)$. An increase of supercurrent velocity would lead to the increasing of supercurrent density, which is given by $J_s = -(2e/m)\left|\varphi\right|^2 \hbar\nabla\varphi(x)$. Yet, the increase of $\nabla\varphi(x)$ cannot go beyond a critical value (in this case a critical velocity

v_c), otherwise it would lead to the inconsistency with a steady state. Therefore, a phase-loss mechanism which would reduce the phase difference is needed to maintain a steady state $v_s < v_c$. The phenomena of phase slip are assumed to occur in the sample where oscillation of the order parameter allows the phase differences to relax by quanta of 2π as it is shown in Fig. 1.4-b. The period of the phase slip center τ_{PSC} is given by $\tau_{PSC} = \pi\hbar/e\bar{V}(t)$ and the frequency of repetition of the phase slip centers is then given by $\omega_{PSC} = 2e\bar{V}(t)/h$, which is the Josephson frequency [10].

The theory of phase slip centers was later developed by Skocpol, Beasley and Tinkham (SBT), also known as SBT model. In their model [11] the applied current is just the superposition of the normal and superconducting current, $I = I_n + I_s$. The superconducting current depends on the behavior of the chemical potential of the Cooper pairs, μ_p, while the normal current depends on the chemical potential of the normal electrons μ. It is assumed that the time-averaged of μ_p is constant along the superconducting strip between points where the phase coherence is lost. It means that μ_p proceeds down a staircase at the center of the phase slips. The order parameter in the middle of the phase slip center is assumed to be zero. The characteristic of the PSC modelled by SBT is shown in Fig. 1.5.

In Fig. 1.5-a, it is shown that the voltage dropped sharply at the core of the PSC and there is no variation in time-averaged value of $\bar{\mu}_p$ inside the superconducting regions (between x_0 and x_1)but only a sharp step at each PSC. On the other hand, the chemical potential of normal electrons varies with time. The

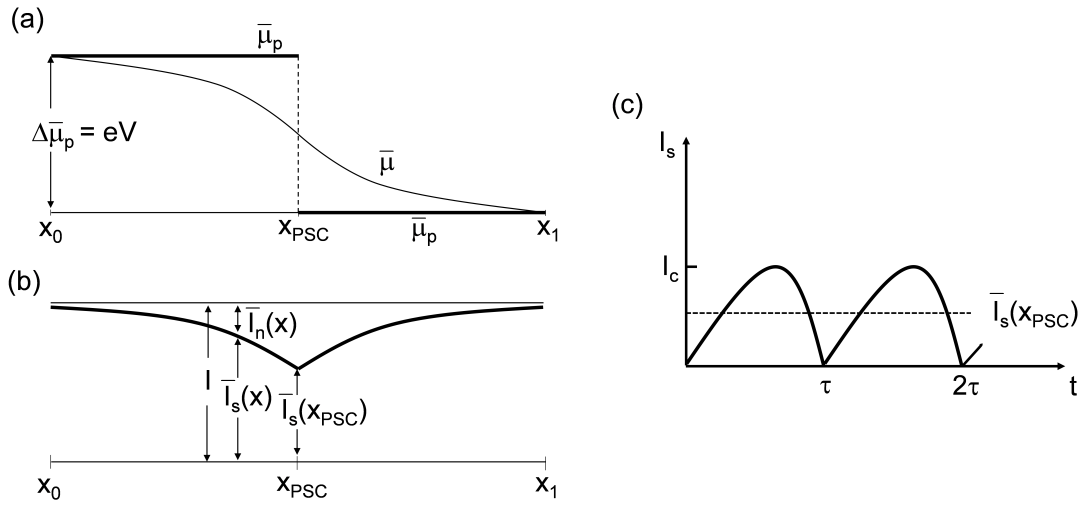

Figure 1.5: Schematic diagram of phase slip centers of SBT model. (a) Time averaged of electrochemical potentials of the Cooper pairs μ_p and quasiparticles μ. (b) Behavior of time averaged supercurrent and normal current along the bridge. The applied current I is drawn only slightly above I_c. (c) The oscillatory of supercurrent in the core of PSC region, with the time averaged supercurrent $I_s \sim I_c/2$ [11].

electrochemical potential difference needed to drive the normal current through a phase slip center is given by

$$V = \Delta\mu/e \approx 2\rho\Lambda\,[j - j_s] = \frac{2\rho\Lambda}{A}\,[I - I_s] \tag{1.6}$$

where A is the local cross sectional area of the bridge, $\rho \sim \rho_n$ is the normal resistivity, and Λ is the diffusion length (essentially the mean free path) of the quasi particles. By modelling the behavior of the chemical potentials using some quantitative formula, SBT came up with a crucial result of the differential resistance, which is given by:

$$\frac{dV}{dj} \approx 2\rho\Lambda \tag{1.7}$$

This result was obtained after assuming that $x_{PSC} - x_1$ and $x_0 - x_{PSC}$ are both much larger than Λ. This then suggests that each PSC contributes a differential of $2\rho\Lambda/A$. SBT estimated that the supercurrent in the core of PSC is about $\bar{I}_s \approx \frac{1}{2} I_c$ (Fig. 1.5-c). The rest of the applied current must then be carried as a normal current. In the non-ideal bridges, the first PSC normally occurs wherever $I_c(x)$ has its minimum because of the nature of the bridges such as strains, variations in cross-sectional area, etc. The next PSC will occur when $I_s(x)$ reaches the $I_c(x)$ at some other point in the bridge. This tends to happen further away from the x_{PSC} when I_s approaches the total current (Fig. 1.5-b). The condition for creation of a new PSC is approximately just $I = I_c(x)$.

1.5 Application of superconductivity: single photon detector

Technological application of superconductors has been increasing rapidly particularly in relation to superconducting magnets, electrical machinery with superconducting coils, superconducting power transmission lines, etc [12]. Recently, superconductor has attracted a lot of attention to its application in the optical communication such as used in superconducting nanowire single photon detector (SNSPD) [13–15]. This emerging technology takes benefit from the phenomenon of hotspot taking place in a narrow superconducting nanowire with a width com-

parable to the coherence length. The basic principle of the SNSPD is shown in Fig. 1.6 [13, 15–18].

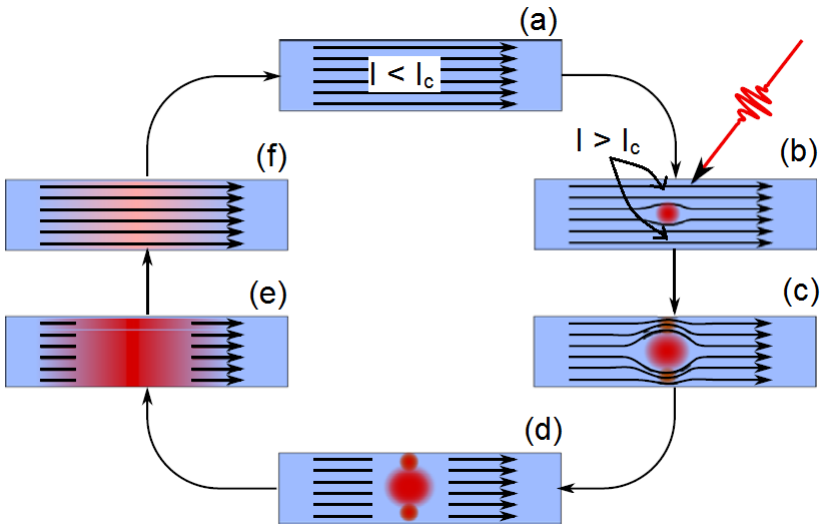

Figure 1.6: The basic principle of SNSPDs showing the formation of resistive state (hot spot) due to the photon absorption (a-b). High current density in the contiguous area exceeds the critical current density resulting in the formation of other hot spots across the wire thus a voltage is generated (c-d). The hot spots expand along the wire and then subside so that the wire return to superconducting state (e-f) [13, 15-18].

SNSPDs rely on a narrow superconducting wire that is biased with a current just below the critical current. When an incoming photon with energy sufficient to disturb the Cooper pairs is absorbed its energy creates a small hot spot of the wire to make transition from the superconducting state to normal state. This causes the current to flow across the normal resistance region and results in an increase of the current density in those contiguous regions. Those contiguous regions then exceed the critical current density and form a normal resistance region all the way across the width of the wire. This small region of the superconducting wire yields a measurable voltage spike that indicates the detection of a single photon.

1.6 Objectives

The aim of this thesis is to study the dissipation mechanisms in a superconducting niobium filament by investigating the voltage response of the filament to a pulse current. The main objectives to be achieved in this study are listed below.

1. To discriminate between phase slip center (PSC) and hot spot (HS) modes using an electrical current pulse technique.

2. To study the effect of the temperature on the two dissipation modes.

3. To study the effect of the temperature on the heat escape time.

CHAPTER 2

DISCRIMINATION BETWEEN PHASE SLIP CENTERS AND HOT SPOTS

In a connected superconducting wire, fed with current from normal leads, perfect conductivity requires that the potential difference V between the ends be zero [3]. It implies that the relative phase difference at two ends holds a constant value, which will depend on the strength of the supercurrent. However, if a resistance appears in the superconducting wire, the averaged phase difference will vary with time resulting in an inconsistency with a steady state. The resolution of this inconsistency is that phase-slips occur, in which case phase coherence is momentarily broken at some point in the superconductor, allowing a phase slip to occur before the phase coherence is reformed. It is known that phase-slip center (PSC) which occurs in response of a superconducting filament to currents larger than

the critical current (I_c). The time-averaged superconducting fraction I_s passes through the filament without dissipation. The total current is the superposition of the normal and superconducting current. The superconducting current I_s is defined by $V = R_u(I - I_s)$ where R_u is the differential resistance, dV/dI, and is independent of the current I [19, 20].

The PSC can be identified with three features. First, the voltage appearing along the superconducting strip is delayed by a time t_d in response to an electrical current pulse. In this respect, the delay time t_d is defined as a time needed to destroy locally the superconductivity. The delay time depends on the applied current. Second, the voltage appearing after a delay time, t_d jumps abruptly and saturates. The temperature reached in the core of PSC is less than the critical temperature.

On the other hand, a hot spot (HS), which is a localized normal zone maintained above the critical temperature by Joule heating, is attributed by a voltage that increases with time after a delay time t_d. However, recent studies have reported that a HS is always preceded by nucleation of PSCs [19, 21–23]. The temperature reached inside a HS is larger than the critical temperature, therefore the current flowing in the HS region is a normal current.

The theoretical explanation of the HS was proposed by Skocpol-Basley-Tinkham (SBT) [24]. In the SBT model, a HS is a localized normal zone generated by Joule heating. Since it is a normal zone, the temperature in those zones is higher than T_c. A sufficient current is required to generate the Joule effect to

maintain the temperature above T_c. We call it the threshold current I_h, not to be confused with the critical current to nucleate the PSC, I_c. In order to maintain a localized HS, this Joule effect per unit volume must compensate not only heat loss to the substrate but also heat conduction along the filament. These are two mechanisms by which the heat generated in a localized HS is transfered [24]. The voltage developed along the HS is determined by its normal resistance.

2.1 Current-temperature phase diagram for different dissipative modes

The nature of dissipative modes can be transcribed in a current-temperature phase diagram showing the temperature dependence of two threshold currents namely I_c and I_h (Fig. 2.1-a). Here, the current $I_c(T)$ and $I_h(T)$ are schematically plotted as functions of bath temperature. The critical current I_c is the pair-breaking threshold, it initiates the nucleation of PSC [3]. However, the current I_h is the minimum threshold current whose Joule effect is sufficient to maintain a localized normal zone above T_c [19].

At temperature very close to T_c, the dependence of I_h on temperature follows a function of $(1 - T/T_c)^{1/2}$. On the other hand, I_c has a form varying from $(1 - T/T_c)^{3/2}$ to $(1 - T/T_c)$ as T/T_c approaches unity [21, 22]. At lower temperatures, I_c increases more abruptly than I_h thus $I_c > I_h$. Whereas, on increasing the bath temperature close to T_c the current I_c decreases more abruptly compared that to I_h

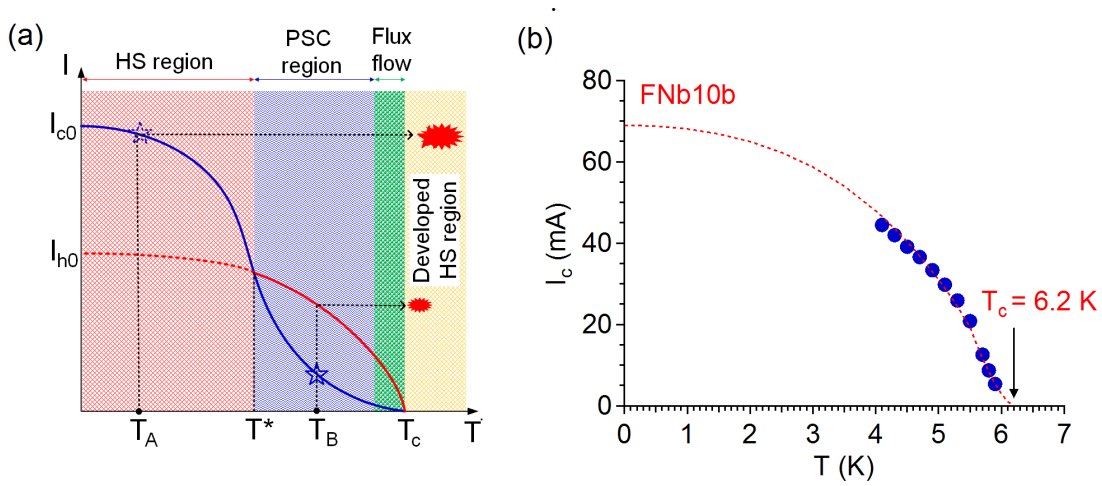

Figure 2.1: (a) Illustration of current-temperature phase diagram showing different dissipative regimes. (b) Measured critical currents of one of our samples, FNb10b, are plotted as a function of temperature. The dashed line is a fitting function using formula [22] of $I_c(T) = I_{c0}(1 + (T/T_c)^2)^{1/2}(1 - (T/T_c)^2)$ and $I_c(T) = C(1 - (T/T_c)^2)^{3/2}$ for temperature range of 0 to 5.5 K and 5.5 to 6.2 K, respectively where coefficients I_{c0} and C, in this fitting, are adjustable constants.

thus resulting in $I_c < I_h$. The current I_c and I_h intersect at a crossing temperature T^*. When the current increases significantly over I_c, the PSC naturally evolves into an ordinary normal zone or hot spot with internal temperature larger than T_c [19, 21].

The schematic diagram of current versus temperature in Fig. 2.1-a which allows to interpret the response of the current steps of increasing amplitude to be explained as the follows: At the bath temperature $T_A < T^*$, on increasing the current the $I_h(T) < I_c(T)$ curve is encountered first but without any response although I_h will not be enough to feed a localized HS on a substrate at temperature T_A. Only when increasing the current and passing the critical current I_c a voltage signal appears. The PSC, after some delay time, is then nucleated as shown in dashed star and is immediately transformed into a hot spot which happens to be

a developing one since $I > I_c > I_h$. The corresponding signal increases linearly with time for constant current bias.

At $T_B > T^*$, the I_c curve is reached first and that defines the proper PSC region ($I_c(T) < I_h(T)$). A current higher than I_c such that $I_c < I < I_h$ creates a PSC whose length is determined by the quasiparticle inelastic diffusion range and is given by $L_n = 2\Lambda = \nu_F(\tau_c\tau_R/2)^{1/2}$, where ν_F is the Fermi velocity, τ_c is the elastic collision time, and τ_R is the transverse inelastic relaxation time [11, 25]. Further increase in current above I_c and once the corresponding I_h is attained the PSC transforms it into a hot spot. At temperature very close to T_c, the dominant dissipative mode is flux flow indicated by the raise of response signal without any delay time.

Measuring of I_c at $T_b < T_c$ is experimentally done by increasing the current until a resistive regime appears indicated by the voltage rise in the filament. It can be done by using a signal generator sending a pulse current to the filament as it will be discussed in the next chapter. The measured I_c of one of our sample as a function of temperature is shown in Fig. 2.1-b. Measuring of I_h at $T_b > T^*$ can be done by increasing the current beyond I_c until the flat voltage of PSC switches into a rising voltage indicating a HS. Measurement of I_h at $T_b < T^*$, on the other hand, is somewhat more complicated. It requires a two-step procedure consisting of one primary pulse generator with a shorter pulse time and another pulse generator with a longer one. A short pulse of intensity larger than I_c is launched creating a rising voltage of HS of same part of the filament. It is followed by a longer

pulse with a current of smaller intensity. If this "return current" is above I_h, an increasing voltage appears corresponds to an expanding HS. However, if the returns current is below I_h, a descending of HS is observed. Then, I_h is determined by the current that maintains the steady level of HS which is the flat voltage on the long pulse.

CHAPTER 3

EXPERIMENTAL SETUP

3.1 Sample fabrication and characterization

3.1.1 Fabrication

Our Nb thin film samples, of 80 nm thick, were deposited at room temperature on sapphire substrates by dc-magnetron sputtering on heated substrates (600^oC) and were patterned to 4-terminal bridges including two lateral probes, 1 mm apart from each other (as shown in the Fig. 3.1), using standard photo-lithograpic processes and ion milling (fabricated by STAR-Cryoelectronics. NM, USA). Contact pads, of about 20 nm in thickness, were made out of gold. The advantages of using gold as a terminal pad cover are to make a contact with low-resistance and long life-time [26]. The width of the sample is determined by a narrow bridge of 800 μm long having three different widths w = 3, 5, and 10 μm. The samples used in the experiment were named according to their widths: FNb3b, FNb3c, and FNb3e (w = 3 μm); FNb5a and FNb5e (w = 5 μm); and FNb10b (w = 10

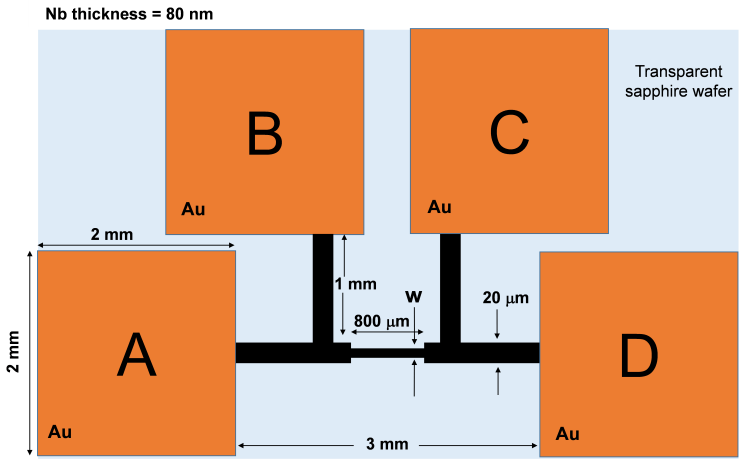

Figure 3.1: Schematic of our Nb samples with the thickness of 80 nm. The samples have three different widths, $w = 3$, 5, and 10 μm

μm)

3.1.2 Characterization

Nb samples were characterized by measuring the resistance as a function of temperature. The R-T measurement were done using a four-point probe technique (see Fig. 3.2-a). Current source KEITH-225 was used to send a current of the

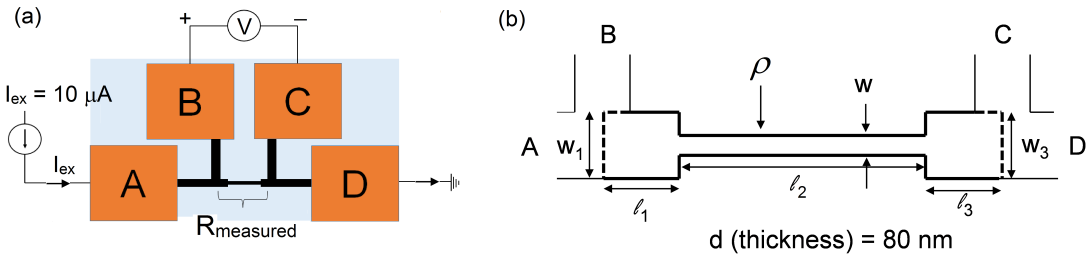

Figure 3.2: (a) Schematic of R-T measurement using four-point probe technique. (b) Schematic of resistivity calculation along the narrow bridge of Nb filament having width w. $l_1 = l_3 = 100$ μm is the length of Nb having width $w_1 = w_3 = 20$ μm. The resistivity of our sample was calculated only for the part of the filament along $l_2 = 800$ μm.

order of micro-ampere, I_{ex}, through the Nb filament from input probe A to the ground via output probe D. The voltage along the filament, V, was measured at the lateral probes B and C using an Agilent-34401 digital multimeter. The measured resistance between these two lateral probes was given by $R_{measured} = V/I_{ex}$. The resistivity of the filament, ρ, was calculated by taking into account only a specific area of narrow bridge having width w (see Fig. 3.2-b). As shown in Fig. 3.2-b, the measured resistance, $R_{measured}$ is given by some part of filament along $l_1 + l_2 + l_3$ and is equal to $R_{measured} = R_1 + R_2 + R_3$. Given $R = \rho\frac{l}{a}$, where l is the length of the measured filament and a is its cross sectional area, then we can write

$$\begin{aligned} R &= R_1 + R_2 + R_3 \\ &= \rho\frac{l_1}{a_1} + \rho\frac{l_2}{a_2} + \rho\frac{l_3}{a_3} \\ &= \rho\left(\frac{l_1}{bw_1} + \frac{l_2}{bw} + \frac{l_3}{bw_3}\right) \\ &= \rho\left(\frac{2l_1}{bw_1} + \frac{l_2}{bw}\right); \quad l_1 = l_3 \quad \text{and} \quad w_1 = w_3 \\ &= \frac{\rho}{bw_1}\left(2l_1 + l_2\frac{w_1}{w}\right) \end{aligned} \tag{3.1}$$

Thus, the resistivity is given by

$$\rho = \frac{Rbw_1}{\left(2l_1 + l_2\frac{w_1}{w}\right)} \tag{3.2}$$

The R-T measurement were performed on three samples: FNb3e, FNb5e, and FNb10b. Some results are presented in Fig. 3.3 for sample FNb3e and FNb5e,

where resistivity is plotted as a function of temperature. For calculation purpose, the values of residual resistivity in the normal state (here we take at $T_b = 10$K) and the transition temperatures of the three samples are listed in Table. 3.1.

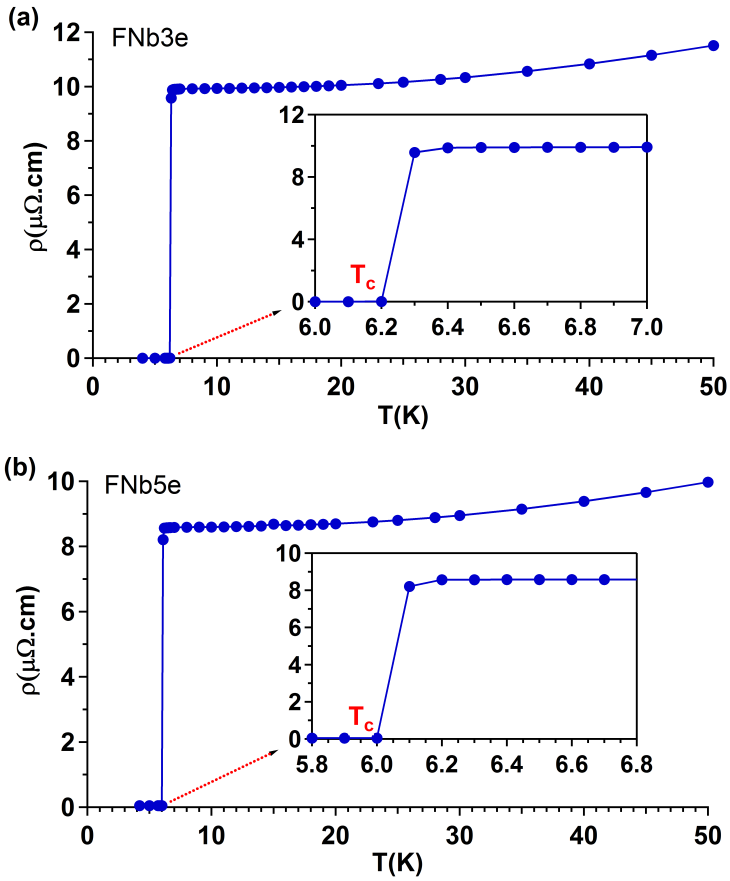

Figure 3.3: Resistivity as a function of temperature for two different samples: (a) FNb3e and (b) FNb5e having widths of $w = 3$ and 5 μm, respectively. The insets show the resistivity of each sample at the vicinity of the critical temperature T_c.

The PSC and HS characterizations were conducted in a helium dewar and a closed-cycled cryostat. For the experiment in the helium dewar, the samples were cooled down to temperature of 4.2 K by immersing it gradually into the helium bath. Whereas, for closed-cycle cryostat measurement, the samples were mounted in the cryostat and kept under vacuum.

Table 3.1: Specifications of the three niobium samples: FNb3e, FNb5e, and FNb10b. Listed are the width w; critical temperature T_c; and normal state resistivity ρ at 10 K

Sample	Width w (μm)	T_c (K)	$\boldsymbol{\rho}$ (10 K) ($\mu\Omega$.cm)
FNb3e	3	6.2	9.57
FNb5e	5	6	8.09
FNb10b	10	6.2	7.35

3.2 Experimental setup

The sketch of experimental setup is shown in Fig. 3.4.

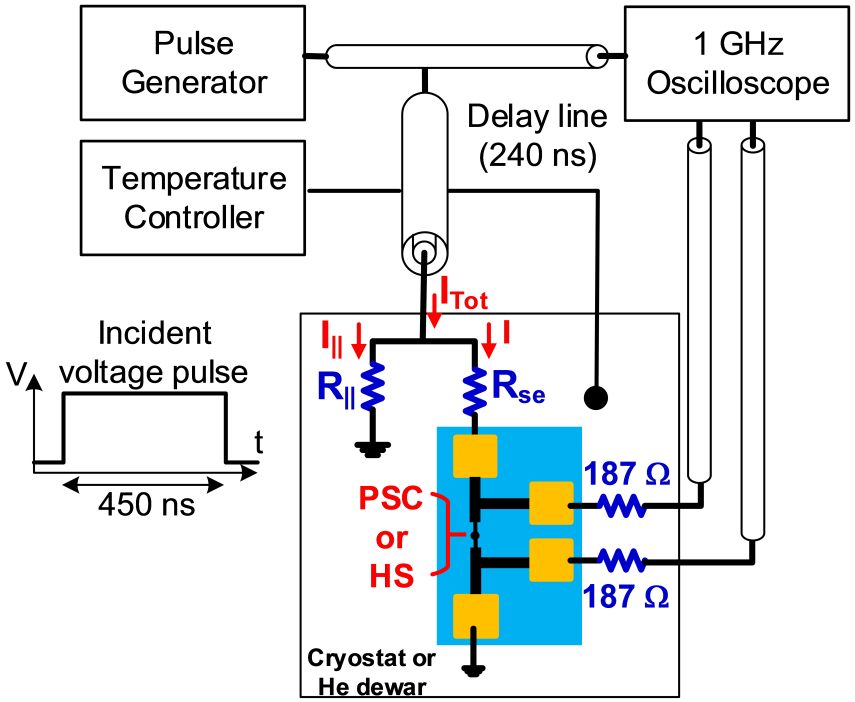

Figure 3.4: Diagram of measurement setup for the pulse measurement. Pulse generator sends current pulses on a 50 Ω coaxial cable to the sample. Large resistances in series and parallel are used to make the reflected pulses vanish. The sample is cooled by either immersing it in a helium dewar or using a closed-cycle cryostat.

An AVETEC (E3A-B) Pulse Generator was used to send electrical pulses of 450 ns duration and 10 kHz repetition rate through 50 Ω coaxial cable to the sample.

A 240 ns delay line was used to separate the incident pulse from the reflected one coming from the sample in time. The voltage response of the sample as well as the incident and reflected pulse were recorded using a 1 GHz oscilloscope (Agilent InviniiVision 6000 Series). The former was measured through lateral electrodes with a 187 Ω resistor connected in series.

The reflected pulse depends on the load given at the end of the coaxial cable (or before the sample) which is determined by a formula $\frac{V_r}{V_i} = \frac{R-Z_o}{R+Z_o}$ where Z_o is the impedance of the coaxial cable (in our setup $Z_o = 50\ \Omega$). If the load at the end of the coaxial cable $R = 0$, the pulse must reflect with the opposite polarity $V_r = -V_i$. When the pulse travel along the coaxial cable to an open end, $R = \infty$, the reflected pulse becomes an identical pulse, $V_r = V_i$. The reflected pulse vanishes when the load at the end of the coaxial cable is equal to its impedance $R = Z_o$. In our measurement, we used a combination of resistance R_{se} and $R_{||}$ such that it is equivalent to the impedance of the coaxial cable which is 50 Ω so that the reflected pulse vanishes. Two combinations of resistance were used *i.e.* $R_{se} = 187\ \Omega$; $R_{||} = 67\ \Omega$ and $R_{se} = R_{||} = 100\ \Omega$. (The incident and reflected pulse signals can bee seen in Appendix A.

To maintain the bias current constant through the sample, a large resistance series R_{se} was used while a resistor $R_{||}$ was mounted in shunt across the combination of R_{se} + Sample. The current flowing through the sample in its superconducting state can be calculated by assuming that the coaxial cable is lossless and the ohmic contact is negligible, and is given by $I = I_{Tot}R_{||}/\big(R_{||} + R_{se}\big)$, where $I_{Tot} = \frac{V_i}{Z}$, the

circuit impedance $Z = 50\ \Omega$ and V_i is an incident voltage. The addition of 187 Ω resistors on the lateral probes was also meant to avoid the current leak into the oscilloscope. Therefore the pulse current will flow through the bridge of the film toward the ground.

The sample was connected to the series resistor by a short thin copper wire adhered to the electrodes terminal using an indium paste. The resistors used in this experiment do not experience much change of value as the temperature cooled down ($\sim$ 5 %). To avoid a thermal leak from the resistors to the sample, a set of thermal anchor was installed and the resistors were greased with some vacuum grease. The samples were mounted either in the closed-cycle cryostat or in the helium dewar. The closed-cycle cryostat was incorporated with a temperature controller to control the bath temperature ranging from 4 K to room temperature. While in the helium dewar, the temperature was fixed at the liquid helium temperature $T_b = 4.2$ K.

CHAPTER 4

RESULTS AND DATA ANALYSIS

This chapter explains the analysis of data obtained from the measurement of voltage response of the samples.

4.1 Nucleation of phase-slip centers and hot spots using electrical current pulse

In the following, the features of current-induced PSCs and HS's will be identified by their voltage behavior versus time which appear after some delay time, t_d. Figure 4.1-a shows the appearance of a PSC depicted in the voltage curves as a function of time of sample FNb5a at temperature $T_b = 4.2$ K. For the current flowing from A to D (see Fig. 3.1) in sample FNb5a, the critical value I_c is 76.1 mA. The value of I_c was determined in practice for the maximum current over

which the voltage response appeared. In other words, I_c is defined as the current producing the longest accessible PSC delay time (commonly 450 ns).

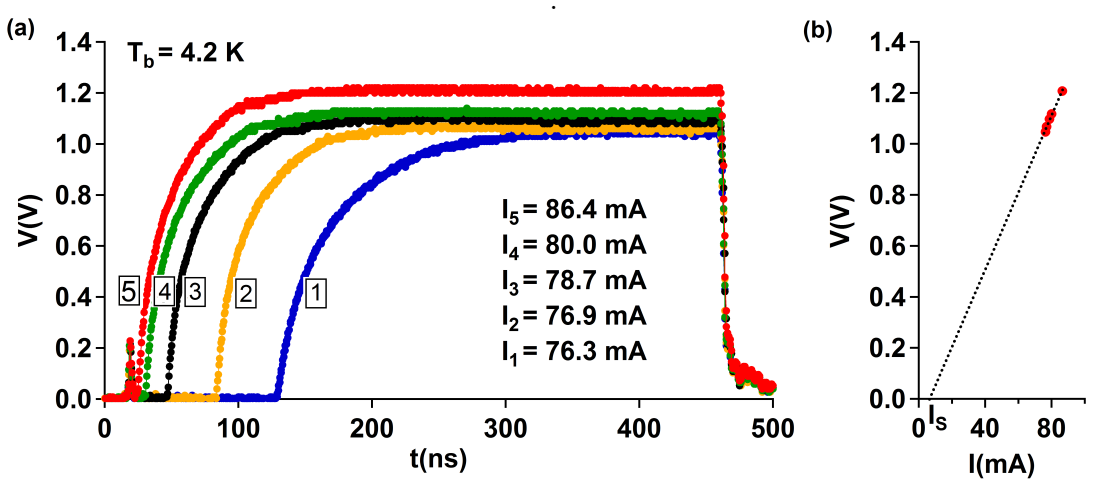

Figure 4.1: (a) Voltage response versus time at different temperatures showing the nucleation of PSC. Here we used $R_{||} = R_{se} = 100\ \Omega$ in the configuration. Measurement were performed on sample FNb5a. (b) The plot of V_{PSC} versus I_{PSC}. The values of the superconducting excess current, I_s are $I_s(4.2\ \text{K}) = 7.1$ mA [27]. (*The original figure is color coded*)

The first voltage response (trace 1) appeared after the bias current was applied slightly above the critical current. It begins with an inductive peak followed by a flat part in an elapsed time t_d and a voltage jump until it saturates. Increasing the applied bias current results in decreasing the delay time t_d until it becomes a very small value to be measured (usually when I exceeds about $2I_c$ [20]). In the meantime, the voltage response increases as the applied current is increased. The physical properties of the sample is found to be at $T_B > T^*$. It is depicted in Fig. 2.1. Some numerical simulations also confirm that the PSC state is characterized by the saturation of the output voltage [27].

The differential resistance of the PSC is extracted from the linear dependence of the PSC‘s voltage versus the applied current. As it is predicted by the PSC‘s theory the extrapolated slope of V_{PSC} *vs* I_{PSC} intercepts the current axis at I_s (Fig. 4.1-b). The PSC was interpreted as an oscillation of the order parameter at the Josephson frequency between between 0 and 1. Therefore, the total current is the sum of the two currents, the normal and superconducting currents. The heat dissipated in this localized zone per unit volume is $\rho I.(I - I_s)/(w \cdot b)^2$, where ρ and I_s are respectively the normal resistivity and the superconducting current [3].

The formation of HS featuring the voltage increase in time is shown in Fig. 4.2. Here we reported the formation of two dissipative regions at different location of the filament. In Fig. 4.2-a, the HS appeared in sample FNb3b at $T_b = 4.2$ K was recorded via probe B and suspected to appear in between probe B’ and C (see inset in Fig. 4.2-b). The HS is also formed after some delay time t_d thus can be quantitatively analyzed in a similar manner. After t_d the output voltage increases rapidly which we relate to the nucleation of PSCs. This process is followed by a slow variation of the voltage increase in time. By raising the bias current, the output voltage increases and the delay time shrinks. The slope of voltage increase corresponds to the expansion velocity of the HS along the filament [28]. The current flowing inside the HS is a normal current and the normal zone expands. The heat generated par unit volume is $\rho I^2/(w \cdot b)^2$ and escapes toward the substrate.

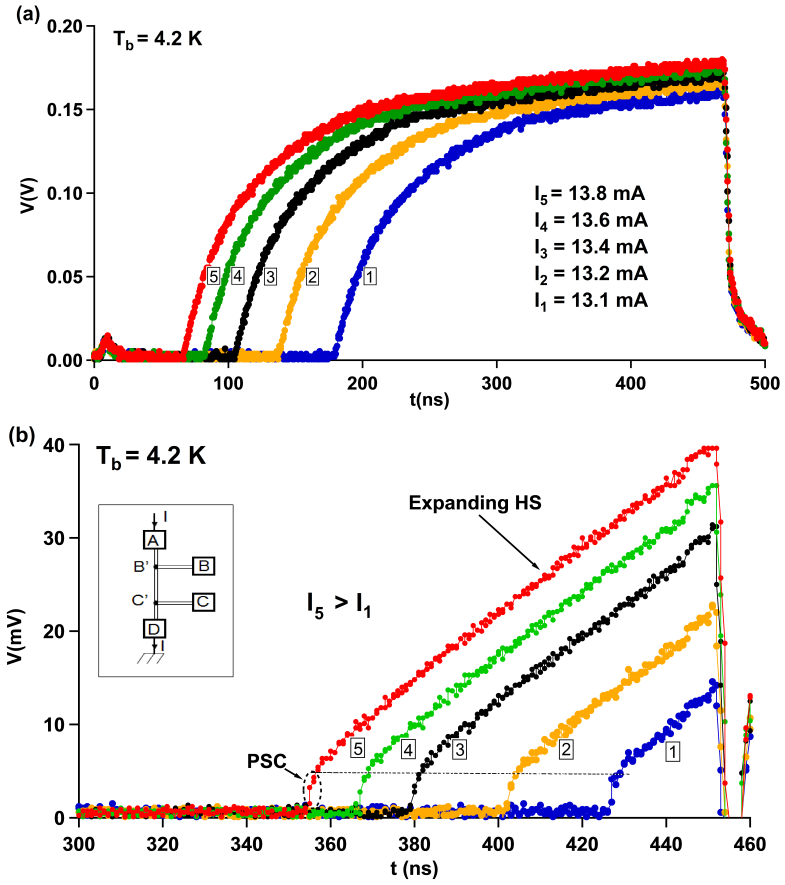

Figure 4.2: Voltage response of sample FNb3b (a) and FNb3c (b) versus time at temperature $T_b = 4.2$ K showing the formation of HS. Here $R_{||} = R_{se} = 100\ \Omega$ for (a) and $R_{||} = 67\ \Omega$ and $R_{se} = 187\ \Omega$ for (b).(*The original figure is color coded*)

More pronounced increase of voltage is shown in sample FNb3c (Fig. 4.2-b). The HS was recorded via lateral probe C. It appears between probe C' and D (see inset in Fig 4.2-b). Much higher applied current than I_c was applied resulting a rapid increase of voltage with time. Here the identification of PSCs is pointed out by a voltage jump at t_d. This behavior can be related to physical properties of sample at $T_b < T^*$ (Fig. 2.1). Here, we can clearly see the transformation of a PSC to an expanding HS.

4.2 Measurement of the heat escape time

In the previous section, it was shown that the delay time shrinks as the current pulse is increased above the critical current. This dependence is shown in Fig. 4.3, where t_d is plotted is a function of the applied current normalized to the critical current (reduced current), I/I_c for three different samples: FNb3e, FNb5e, and FNb10b at 2 different temperatures for each sample (plotting at other temperatures can be seen in Appendix B). The time t_d is measured as being elapsed time from the initial rising edge of the inductive peak until the voltage arises associated with the resistive state. The signal of the output voltage was found to have a jitter. Due to this unstable signal, the value of t_d was measured by taking the averaged signal output from the oscilloscope.

In order to explain these data, we follow the Pals and Walter derivation of the time dependent Ginzburg-Landau (TDGL) theory which describes the behavior of time-dependent order parameter [29]. Solving the TDGL equation in one-

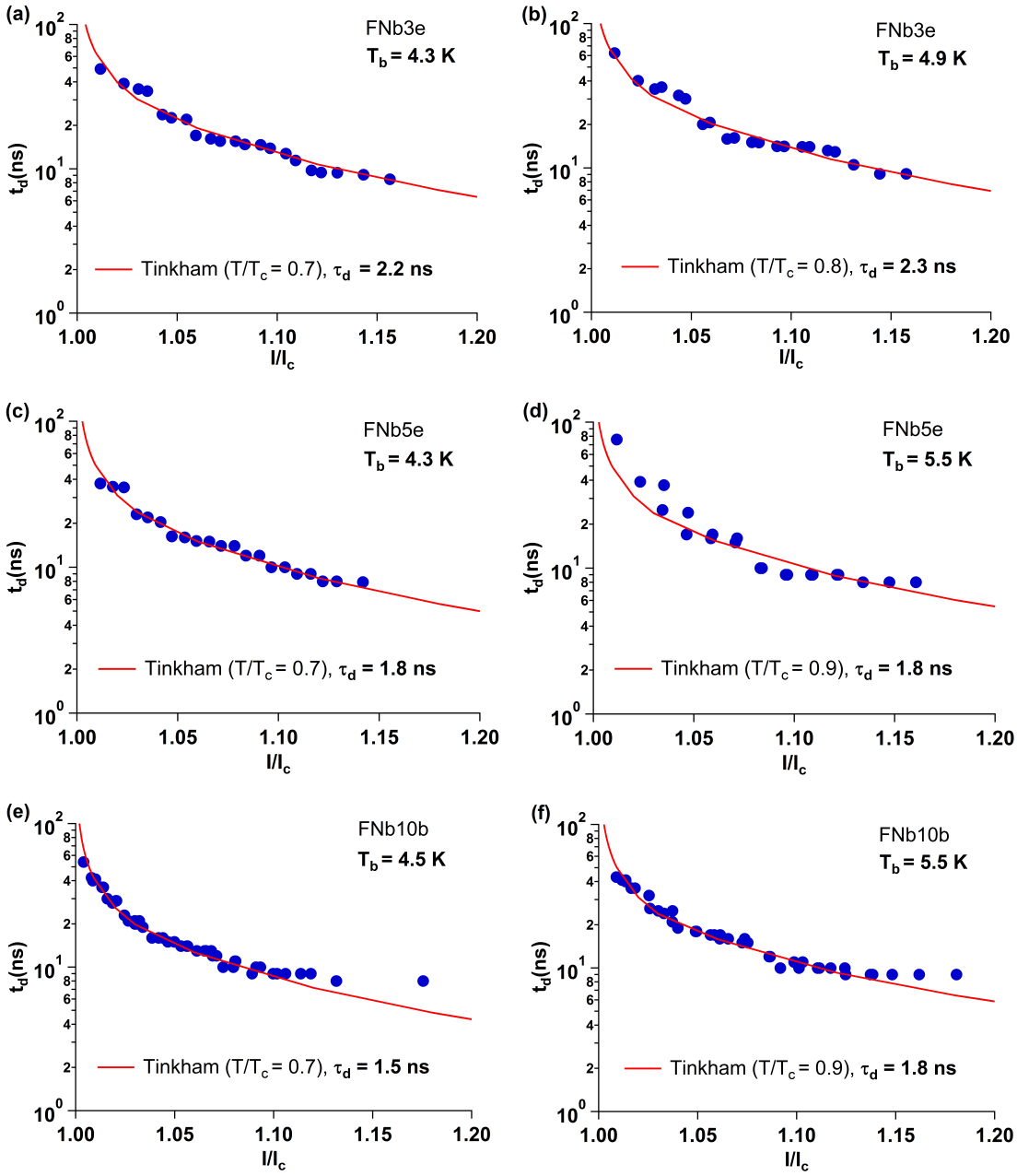

Figure 4.3: Delay time versus ratio of the applied current to the critical current I_c at different temperatures in sample FNb3e (a & b), FNb5e (c & d), and FNb10b (e & f). The solid lines are the Tinkham's fitting functions for different T/T_c's with the prefactors τ_d (see in the figures)

dimensional case (neglecting the space dependence) leads to a simplified equation for the order parameter

$$\frac{df}{dt} = \frac{1}{2\tau_d}\left(1 - f^2 - \frac{4j^2}{27f^4}\right) \tag{4.1}$$

where f is the normalized modulus of the order parameter, j is the reduced current and τ_d is initially interpreted as gap-relaxation time. This equation implies that, for $j < j_c$, f approaches a limiting constant value f_{eq} found in the equilibrium state ($f \sim 1$) [3]. When j is slightly above j_c, f starts to decrease very slowly until it passes f_{eq} then the rate of decrease of f increases as f falls further approaching 0. Assuming that t_d is the time when the order parameter f goes to 0, Eq. (4.1) can be written in integral form [29]:

$$t_d\,(I/I_c) = \tau_d \int_0^1 \frac{2f^4 df}{(4/27)\,(I/I_c)^2 - f^4 + f^6} \tag{4.2}$$

where t_d is an adjustable parameter to fit the data.

The Pals and Walter equation (4.2) is in good agreement with experimental results especially for currents slightly above I_c and temperatures near the T_c. However, a significant deviation was found for current significantly higher than I_c and temperatures far from T_c [20]. It was pointed out by Tinkham [30], who treated the case of arbitrarily fast-variation of energy gap and came up with a formula for t_d having the same form as Eq. (4.2) with the numerator in the

integrand replaced by:

$$2f^4 + 1.65f^5 - 0.5(I/I_c)^2 \tag{4.3}$$

where t_d is a function of two variables, T/T_c and I/I_c. The adjustable time parameter τ_d was interpreted as the effective gap relaxation time [29]. It is in close connection with the electron-phonon relaxation time τ_{ep}.

Upon the nucleation of normal region in the superconducting wire, the electron and phonon are in charge of the heat conduction along the filament. In the mean-time, the heat dissipation transfered to the substrate is mainly conducted by the phonon energy. Let E_e and E_p be the electron and phonon energies dissipated in this process, respectively, the power dissipation along the filament can be written as:

$$P_f = \frac{\int C_e dT + \int C_p dT}{\tau_d} \tag{4.4}$$

where C_e and C_p are the specific heat of electron and phonon, respectively. τ_d is the characteristic time deduced from the Eq. (4.2) For the heat transfer by phonons escaping to the substrate, the power dissipation is given by:

$$P_s = \frac{\int C_p dT}{\tau_{esc}} \tag{4.5}$$

Assuming the power dissipated through the filament and to the substrate are equally the same during the dissipation process, then, in the linear approximation,

the phonon escape time can be deduced by equating Eq. (4.4) and Eq. (4.5) resulting in:

$$\frac{C_e + C_p}{C_p} = \frac{\tau_d}{\tau_{esc}} \tag{4.6}$$

or

$$\tau_{esc} = \tau_d(\frac{C_p}{C_e + C_p}) \tag{4.7}$$

For sample FNb3e (Fig. 4.3-a & -b), the fitting function of Eq. (4.1, 4.3) gives $\tau_d = 2.2$ ns and 2.3 ns at temperatures $T_b = 4.3$ K and 4.9 K, respectively. For wider sample, namely FNb5e, τ_d is found to be slightly smaller which is 1.8 ns at temperatures $T_b = 4.3$ K and 5.5 K (Fig. 4.3-c & -d). A smaller value of τ_d than that of FNb5e is found on sample FNb10b, whose w is larger than that of FNb5e.

4.3 Temperature dependence of the heat escape time

In order to study the temperature behavior of the heat escape time τ_{esc}, we plotted τ_d deduced from the Eq. (4.2) as a function of temperature for samples with different widths (Fig. 4.4). The measurement of t_d was done three times for each sample resulting in a data dispersion with typical uncertanty of 5 %. The result shows that the τ_d tends to be constant as the bath temperature increases up to

5.5 K. Unfortunately, we were not able to get the data for the temperatures close to T_c due to weak signals.

Besides the acoustic mismatch between two lattices and the defects of the interface, which reduce the transmission factor η almost independently of temperature, another cause must be sought in *phonon-phonon interactions*, which are favored by the increase in the temperature. An increase in temperature acts in several ways: i) the average phonon energy ($hf \simeq 2.8$ kT) reaches a domain of rounding of the dispersion relation (hf *vs.* $q = 2\pi/\lambda$, where q is a phonon wave vector). That allows many phonon channels decay as compared to the linear f *vs.* q. ii) the phonons are simply more numerous and impede one another, causing phonon transport to become diffusive rather than ballistic. This slows down the evacuation of heat from the film. In niobium films, phonon are still in the Debye regime at temperature $T \simeq T_c/2 \simeq 4.2$ K. The dispersion relation is linear and phonon-phonon scattering is only a few.

4.4 The temperature at the center of the dissipation

As we mentioned earlier in previous chapter, the temperature inside a hot spot is higher than T_c. To estimate the value of this temperature, we follow an approach developed by Maneval *et al.* [23] to model the temperature profil of hot spots. First, let us define $J_u(T_b)$ as the current density that would exactly maintain T_c

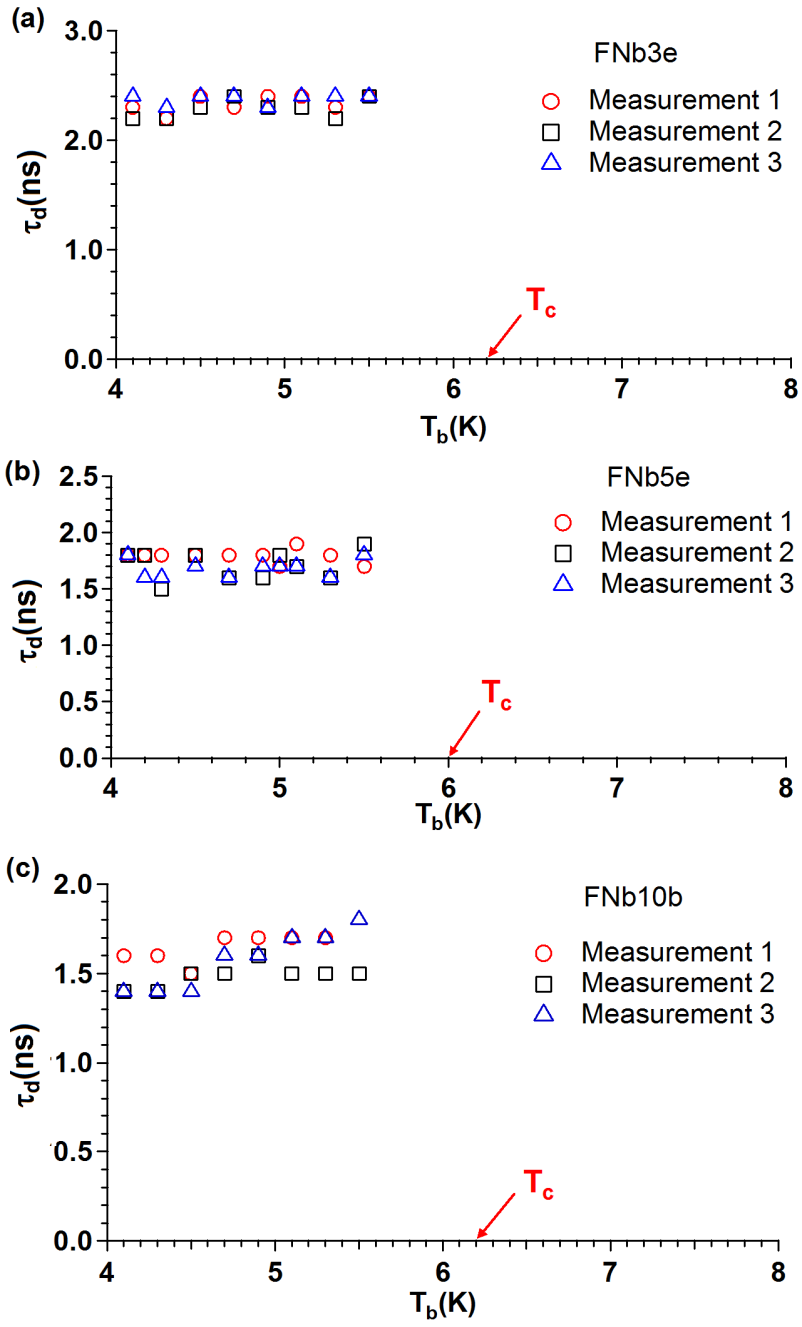

Figure 4.4: Heat escape time τ_d as a function of temperature of samples: (a) FNb3e, (b) FNb5e and (c) FNb10b.

in a uniformly heated film in contact with a substrate at bath temperature T_b, so that:

$$\rho J_u^2 = \frac{C}{\tau_{esc}}(T_c - T_b) \tag{4.8}$$

where C is the uniform volumetric heat capacity.

Sustaining an isolated hot spot upon a substrate at temperature T_b needs more current density $J_h(T_b)$ due to the heat conduction across the healing boundaries [11]. The value of $J_h(T_b)$ needed is approximately equal to $\sqrt{2}J_u(T_b)$ [21, 25]. Close to T_c, the dependence of any of two current densities J_u and J_h upon T_b follows a parabolic curve. However, far below T_c it is more favorable to use the blackbody radiation power density $\sigma_\varphi(T^4 - T_b^4)$ per unit film area, where σ_φ is the Stefan constant appropriate to acoustic phonons, to represent the heat loss through the interface with the substrate. Combining the phonon specific heat in the Debye model $C_\varphi = \beta T^3$ and the independent phonon escape time τ_{esc} leads to $\sigma_\varphi = \alpha/4T_c^3 = b\beta/4\tau_{esc}$, where β is the constant in Debye regime. This implies that a blackbody emission power is tangentially consistent with Eq. (4.8) in the limit $T \to T_b$. The temperature inside the HS core is then estimated using

$$\frac{\rho I^2}{w^2 b^2} = \frac{\sigma_\varphi}{b}(T_M^4 - T_b^4) = \frac{\beta}{4\tau_{esc}}(T_M^4 - T_b^4) \tag{4.9}$$

Here, $I = wbJ_u$ and T_M is the temperature reached in the core of HS. The calculated results of T_M for various samples are listed in Table 4.1. The value of

.

Table 4.1: Estimation of HS core temperature T_M in sample FNb10b for different values of applied current and bath temperature T_b.

Sample	T_b (K)	I (mA)	$\boldsymbol{\tau_{esc}}$ (ns)	T_M (K)
FNb10b	4.5	39.3	0.48	18.63
FNb10b	5.1	29.8	0.48	16.25

β for Nb is taken from the literature, where β(Nb) = 135 μJ$mol^{-1}K^{-4}$ = 12.3 J$m^{-3}K^{-4}$ [19].

CHAPTER 5

CONCLUSIONS

We have studied the dissipative machanisms in superconducting niobium strips at different temperatures using a current pulse technique. The pulse current was sent using a signal generator to the sample via a 50 Ω coaxial cable. A 250 ns delay line was used to separate the incident pulse from the reflected one. Before reaching the sample, the current passed through a set of resistors with equivalent resistance equal to the coaxial cable impedance in order to make the reflected pulse vanish. A larger resistance was put in series to the sample so that the current was maintained to a constant value when the voltage appeared in the sample as measured by oscilloscope via lateral probes with 187 Ω resistors connected in series.

The resistance measurements as a function of temperature have yielded critical temperatures of the samples T_c between 6 and 6.2 K. Applying a current below the critical current at temperatures below T_c keeps the sample in the superconducting state indicated by a zero voltage. The voltage appears in the sample after the

applied current becomes larger than the critical current, this is observed to happen after some delay time, t_d. The appearance of voltage indicating the formation of resistive state is discriminated between the PSC and HS. Besides the appearance after some delay time, both dissipation modes are characterized by their output voltage features. The former, is characterized by a voltage jump and is found to be dynamically stable in time. The latter, on the other hand, is characterized by the linear increase of the output voltage with time. It is shown that the formation of HS is preceded by the nucleation of the PSC. The delay time for the formation of the resistive states decreases by increasing the applied current at a fixed temperature.

We have shown that the delay time as a function of the reduced current I/I_c is well fitted using a simplified time-dependent Ginzburg-Landau equation. From this relation, we are able to deduce the heat escape time as due to heat transfer from the film to the substrate. We have shown, for niobium films, that the heat escape time is independent of the temperature in the Debye regime. In addition, we have estimated the temperature reached inside the resistive states. For HS, the result appears to be consistent with the prediction for $T_{HS} > T_c$.

APPENDIX A

INCIDENT AND REFLECTED PULSE

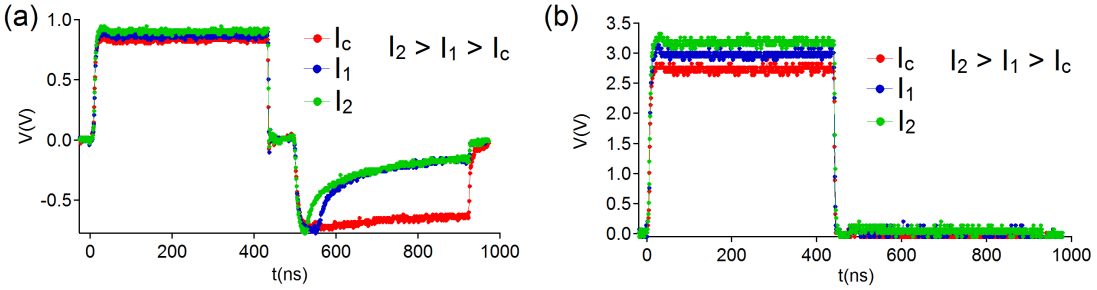

Figure A.1: Voltage versus time measured at probe A showing the incident and different reflected signals. (a) The pulse currents were sent directly to the sample without a resistors circuit. (b) The pulse currents passed a set of resistor circuit with an equivalence resistance of 50 Ω prior to the sample causing the reflected pulse vanishes. *The original figure is color coded*

APPENDIX B

MORE RESULTS AND DATA ANALYSIS

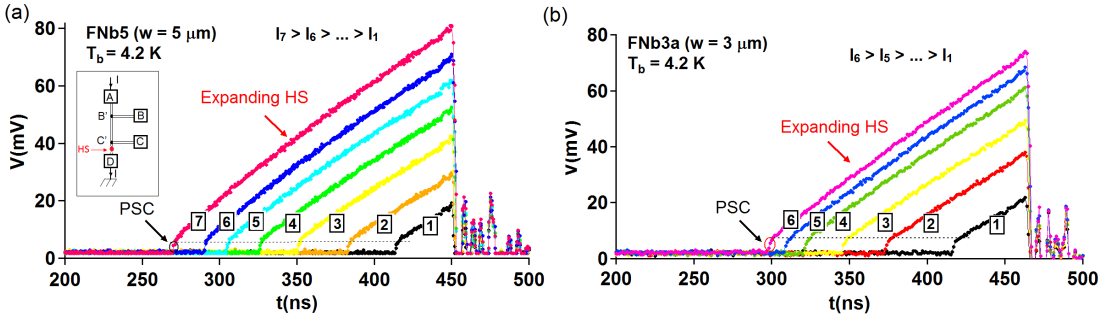

Figure B.1: Voltage versus time of sample FNb5a (a) and FNb3a (b) showing the expansion of HS' preceded by the nucleation of PSC's at temperature of $T_b = 4.2$ K. The hotspots on both sample appear in between point C' and D (see inset in (a)).

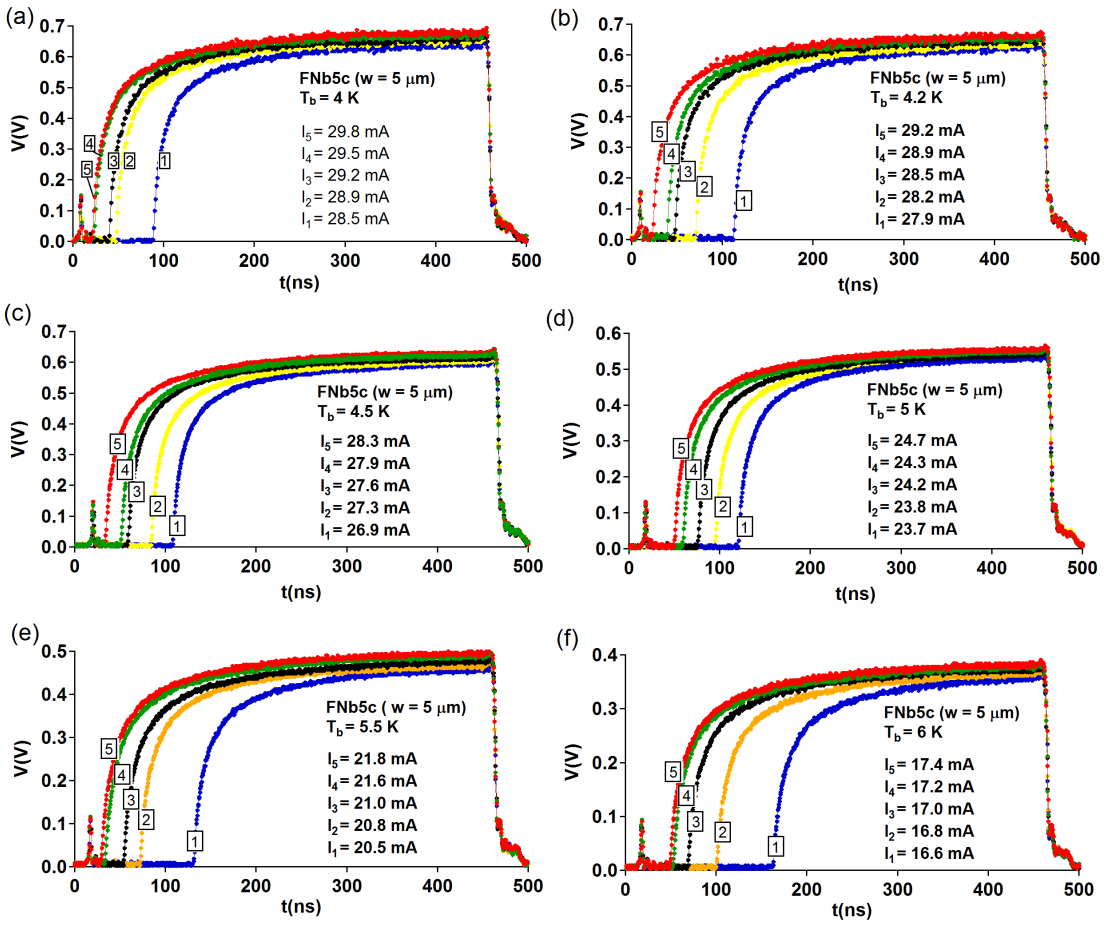

Figure B.2: Voltage versus time of another niobium sample namely FNb5c having width $w = 5$ μm showing the formation of HS. The measurements were taken at different temperatures: (a) 4 K, (b) 4.2 K, (c) 4.5 K, (d) 5 K, (e) 5.5 K, and (f) 6 K.

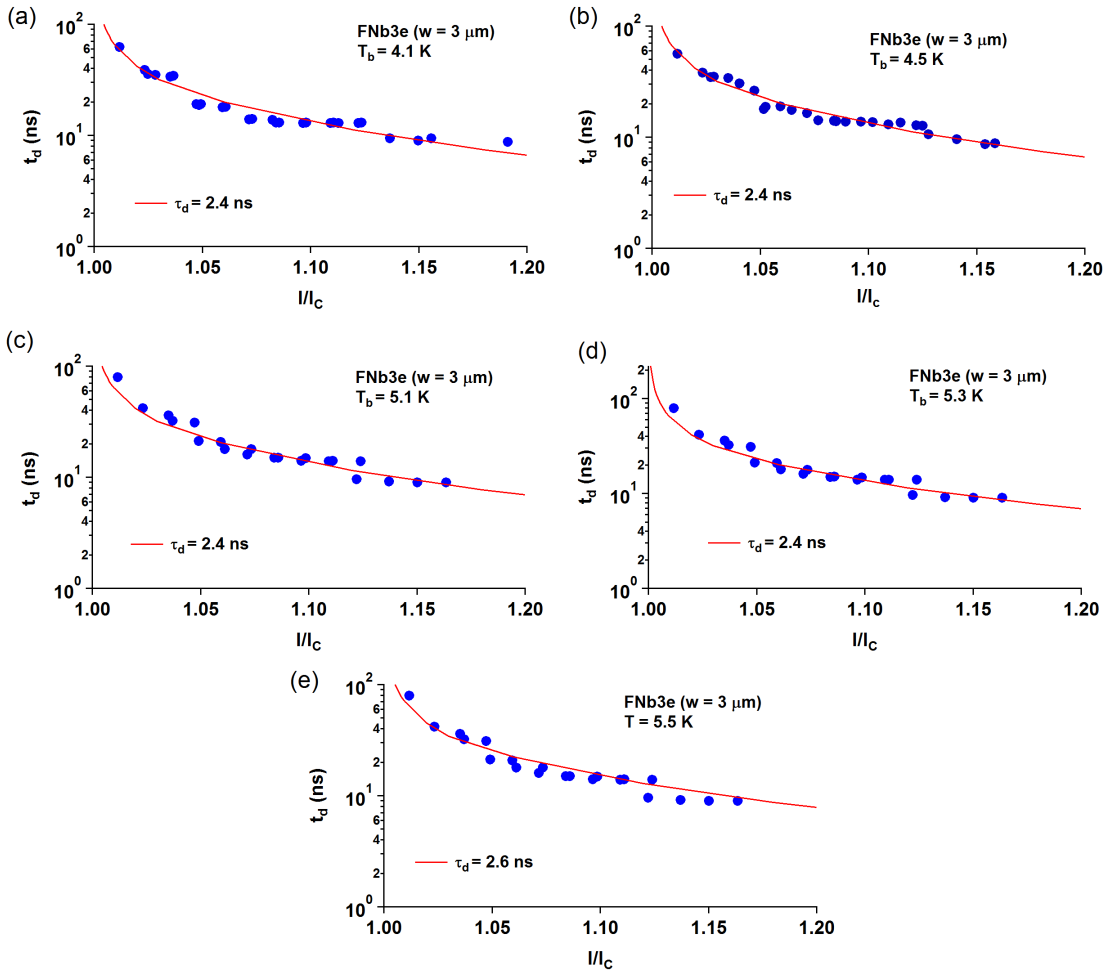

Figure B.3: Delay time t_d as a function of reduced current I/I_c for sample FNb3e at different bath temperatures. The solid lines are the Tinkham's fitting functions with prefactors τ_d.

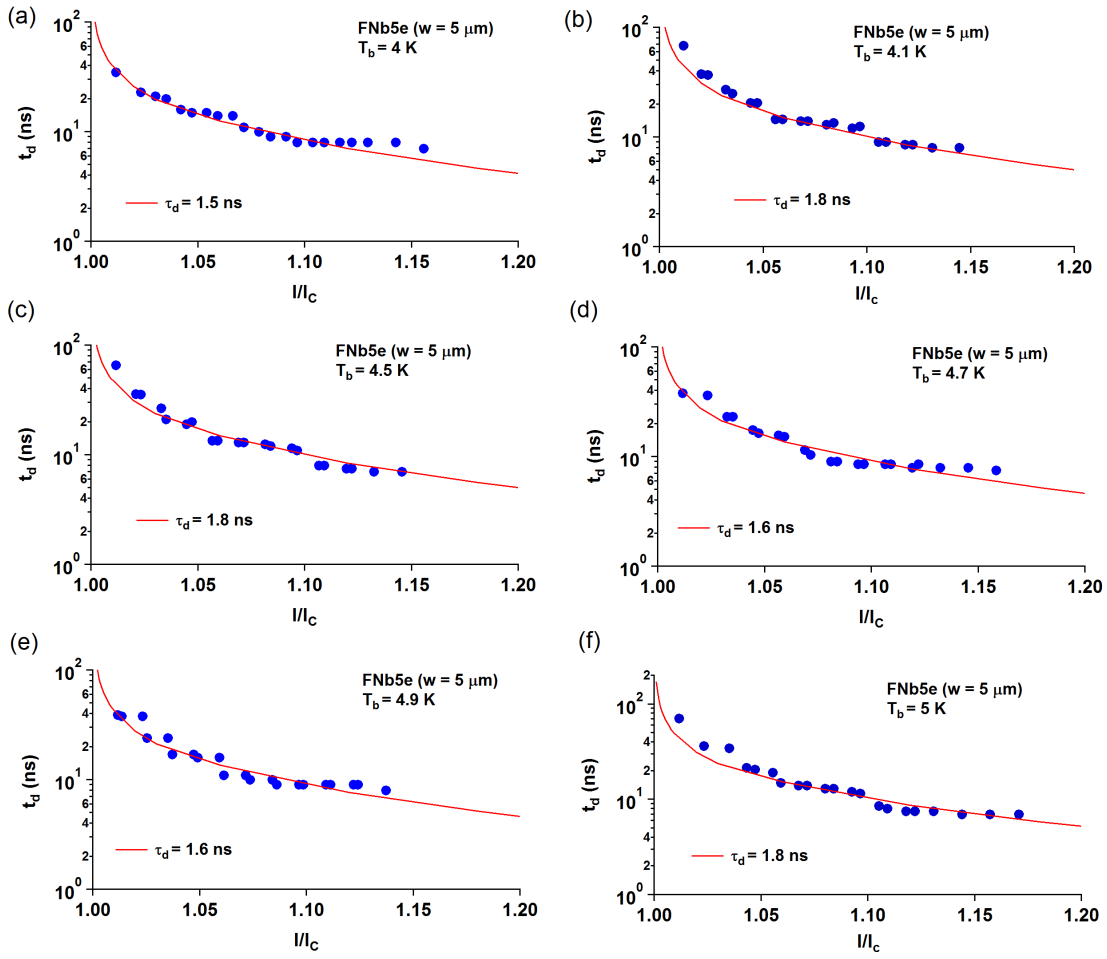

Figure B.4: Delay time t_d as a function of reduced current I/I_c for sample FNb5e at different bath temperatures. The solid lines are the Tinkham's fitting functions with prefactors τ_d.

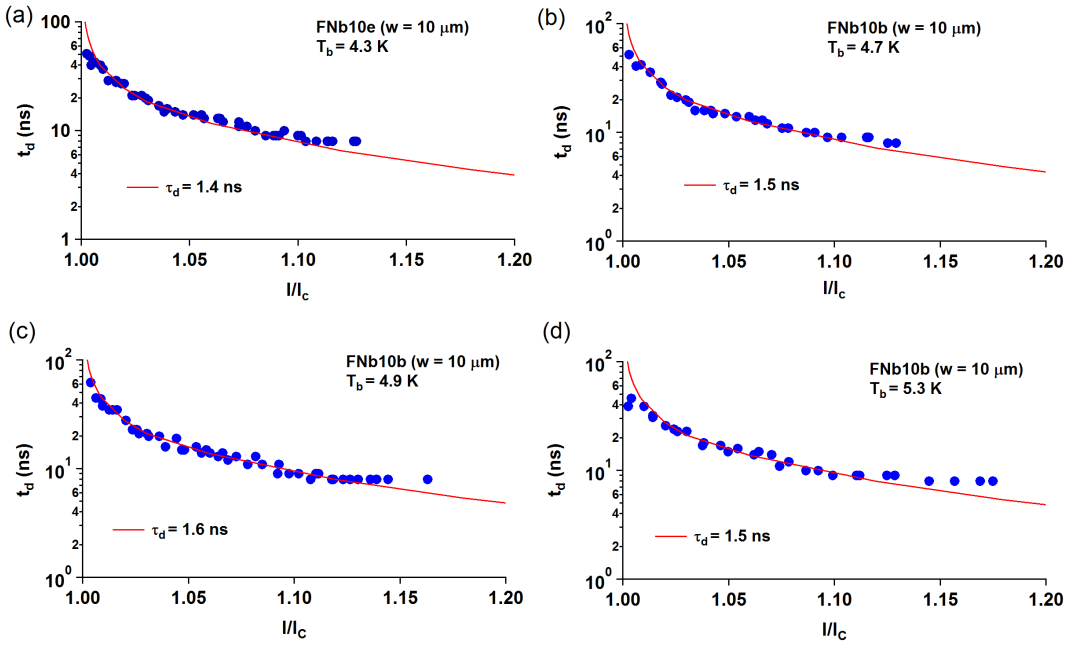

Figure B.5: Delay time t_d as a function of reduced current I/I_c for sample FNb10b at different bath temperatures. The solid lines are the Tinkham's fitting functions with prefactors τ_d.

REFERENCES

[1] C. Enss and S. Hunklinger, *Low-Temperature Physics.* Berlin: Springer-Verlag Berlin Heidelberg, 2005.

[2] E. A. Lynton, *Superconductivity.* London: Mutheun, 1962.

[3] M. Tinkham, *Introduction to superconductivity.* Singapore: McGraw-Hill, 1996.

[4] J. Bardeen, L. N. Cooper, and J. R. Schrieffer, "Theory of superconductivity," *Phys. Rev.*, vol. 108, pp. 1175–1204, 1957.

[5] W. W. Webb and R. J. Warburton, "Intrinsic quantum fluctuations in uniform filamentary superconductors," *Phys. Rev. Lett.*, vol. 20, no. 9, p. 461, 1968.

[6] J. D. Meyer, "Spannungsstufen in denu (t)-übergangskurven undu (i)-kennlinien stromtragender zinn-whisker," *App. Phys.*, vol. 2, no. 6, pp. 303–320, 1973.

[7] J. S. Langer and V. Ambegaokar, "Intrinsic resistive transition in narrow superconducting channels," *Phys. Rev.*, vol. 164, no. 2, pp. 498–510, 1967.

[8] W. J. Skocpol, M. R. Beasley, and M. Tinkham, "Self-heating effects in voltage-biased superconducting microbridges," in *B. Am. Phys. Soc.*, vol. 18, no. 3, 1973, pp. 302–302.

[9] W. A. Little, "Decay of persistent currents in small superconductors," *Phys. Rev.*, vol. 156, no. 2, pp. 396–403, 1967.

[10] T. J. Rieger, D. J. Scalapino, and J. E. Mercereau, "Time-dependent superconductivity and quantum dissipation," *Phys. Rev. B*, vol. 6, pp. 1734–1743, 1972.

[11] W. J. Skocpol, M. R. Beasley, and M. Tinkham, "Phase-slip centers and nonequilibrium processes in superconducting tin microbridges," *J. Low Temp. Phys.*, vol. 16, no. 1-2, pp. 145–167, 1974.

[12] A. W. B. Taylor, *Superconductivity.* London: Wykeham Publications, 1970.

[13] C. M. Natarajan, M. G. Tanner, and R. H. Hadfield, "Superconducting nanowire single-photon detectors: physics and applications," *Supercond. Sci. Tech.*, vol. 25, no. 6, p. 063001, 2012.

[14] R. H. Hadfield, "Single-photon detectors for optical quantum information applications," *Nat. Photonics*, vol. 3, no. 12, pp. 696–705, 2009.

[15] M. D. Eisaman, J. Fan, A. Migdall, and S. V. Polyakov, "Invited review article: Single-photon sources and detectors," *Rev. Sci. Instrum.*, vol. 82, no. 7, p. 071101, 2011.

[16] G. N. Goltsman, O. Okunev, G. Chulkova, A. Lipatov, A. Semenov, K. Smirnov, B. Voronov, A. Dzardanov, C. Williams, and R. Sobolewski, "Picosecond superconducting single-photon optical detector," *Appl. Phys. Lett.*, vol. 79, no. 6, 2001.

[17] A. D. Semenov, G. N. Goltsman, and A. A. Korneev, "Quantum detection by current carrying superconducting film," *Physica C*, vol. 351, no. 4, pp. 349–356, 2001.

[18] J. K. Yang, A. J. Kerman, E. A. Dauler, V. Anant, K. M. Rosfjord, and K. K. Berggren, "Modeling the electrical and thermal response of superconducting nanowire single-photon detectors," *IEEE Trans. on Appl. Supercond.*, vol. 17, no. 2, pp. 581–585, 2007.

[19] K. Harrabi, "Hotspot temperatures reached in current-driven superconducting niobium filaments," *J. Supercond. Nov. Magn.*, vol. 26, no. 5, pp. 1865–1868, 2013.

[20] F. S. Jelila, J.-P. Maneval, F.-R. Ladan, F. Chibane, A. Marie-de Ficquelmont, L. Méchin, J.-C. Villégier, M. Aprili, and J. Lesueur, "Time of nucleation of phase-slip centers in $YBa_2Cu_3O_7$ superconducting bridges," *Phys. Rev. Lett.*, vol. 81, pp. 1933–1936, 1998.

[21] F.-R. Ladan, K. Harrabi, M. Rosticher, P. Mathieu, J.-P. Maneval, and C. Villard, "Current-temperature diagram of resistive states in long super-

conducting niobium filaments," *J. Low Temp. Phys.*, vol. 153, no. 3-4, pp. 103–122, 2008.

[22] K. Harrabi, F.-R. Ladan, V. D. Lam, J.-P. Maneval, J.-F. Hamet, J.-C. Villégier, and R. W. Bland, "Current-temperature diagram of resistive states in long superconducting $YBa_2Cu_3O_7$ strips," *J. Low Temp. Phys.*, vol. 157, no. 1-2, pp. 36–56, 2009.

[23] J. P. Maneval, K. Harrabi, F. Chibane, M. Rosticher, F. R. Ladan, and P. Mathieu, "Temperature profile of hotspots in narrow current-biased superconducting strips," *IEEE Trans. on Appl. Supercond.*, vol. 23, no. 3, p. 2200604, 2013.

[24] W. J. Skocpol, M. R. Beasley, and M. Tinkham, "Self heating hotspots in superconducting thinfilm microbridges," *J. Appl. Phys.*, vol. 45, no. 9, pp. 4054–4066, 1974.

[25] K. Harrabi, N. Cheenne, F. Chibane, F. Boyer, P. Delord, F.-R. Ladan, and J.-P. Maneval, "Thermal boundary resistance of $YBa_2Cu_3O_7$ on MgO films deduced from the transient V(I) response," *Supercond. Sci. Tech.*, vol. 13, no. 8, pp. 1222–1226, 2000.

[26] J.-P. Maneval, F.-R. Ladan, J.-C. Villégier, V. D. Lam, and P. H. Khi, "Excitation of resistive states in superconducting films by using electrical and light pulses," *J. Kor. Phys. Soc.*, vol. 52, no. 5, pp. 1641–1644, 2008.

[27] G. Berdiyorov, K. Harrabi, F. Oktasendra, K. Gasmi, A. I. Mansour, J.-P. Maneval, and F. M. Peeters, "Dynamics of current-driven phase-slip centers in superconducting strips," *Phys. Rev. B*, vol. 90, no. 5, p. 054506, 2014.

[28] K. Harrabi, "Temperature elevation of current-driven phase-slip centers in $YBa_2Cu_3O_7$ strips," *J. Supercond. Nov. Magn.*, vol. 28, pp. 573–577, 2014.

[29] J. A. Pals and J. Wolter, "Measurement of the order-parameter relaxation in superconducting Al-strips," *Phys. Lett. A*, vol. 70, no. 2, pp. 150–152, 1979.

[30] M. Tinkham, *Non-equilibrium superconductivity, phonons and Kapitza boundaries*. New York: Plenum-in cooperation with NATO Scientific Affairs Division, 1981.

Vita

Name	:	Fandi Oktasendra
Nationality	:	Indonesian
Date of Birth	:	October 24, 1988
Email	:	*fandifoks@gmail.com*
Permanent Address	:	Suliki Baruh, Lima Puluh Kota Regency, West Sumatera Province, Indonesia 26255
Education Background	:	**Sept 2006–Jan 2011** B.Sc. in Physics from Institut Teknologi Bandung, Bandung, Indonesia

List of Publication(s) :

1. G. Berdiyorov, K. Harrabi, **F. Oktasendra**, K. Gasmi, A. I. Mansour, J. P. Maneval, and F. M. Peeters, *Dynamics of current-driven phase-slip centers in superconducting strips*, Phys. Rev. B **90**, 054506 (2014) (7 pages)